Characterization of a D-band Active Transmitarray System for Efficient Point-to-Point Links

Francesco Foglia Manzillo *, José Luis González-Jiménez *, Abdelaziz Hamani *, Alexandre Siligaris *, Antonio Clemente *
*CEA - Leti, Univ. Grenoble Alpes, F-38000 Grenoble, France,
{francesco.fogliamanzillo, joseluis.gonzalezjimenez}@cea.fr

***Abstract*—We present the design and characterization of an innovative D-band transmitting antenna system. It comprises an active focal-plane array with two separate antennas which radiate two different signals, with adjacent bands, generated by an integrated circuit, and a flat discrete lens. The lens is designed to form a high-directivity broadside beam in both bands, i.e. from 139.3 GHz to 156.6 GHz. The use of two narrowband signals enhances the spectral efficiency and power consumption. Measurements show a remarkable improvement of transmitted power with respect to similar transmitters performing channel aggregation with guided components. The effective isotropic radiated power is higher than 25 dBm in a relative bandwidth of 11% and attains a peak value of 30.5 dBm. The measured radiation patterns are stable with frequency in each of the two sub-bands. The estimated antenna gain of the system (about 26 dBi) is in tight agreement with numerical data.**

***Index Terms*—millimeter-wave antennas, active antennas, antennas-in-package, lens antennas.**

I. Introduction

The wide available spectrum between 100 GHz and 300 GHz has recently boosted the research on novel high-gain antenna and circuit architectures for the realization of high-data-rate sub-THz wireless links. The significant path loss at these frequencies demands that the transmitter (TX) has a high effective isotropic radiated power (EIRP) over a quite large fractional bandwidth. Relatively small phased arrays of printed elements achieving EIRP values up to 32 dBm have been recently reported at D-band [1]–[3]. However, most of these designs operate over relative bandwidths $< 10\%$. Moreover, their relevant energy consumption and interconnect losses make them hardly scalable.

Space-fed antenna architectures, such as shaped lens antennas [4], [5], reflectarrays [6], and transmitarrays (TAs) [7]-[9], may reduce the overall power consumption with respect to phased arrays, yet providing high EIRP values. Indeed, the primary sources of a space-fed antenna can be excited by a single or a few TX circuits. Nevertheless, the realization of wideband and efficient TX modules is still an open challenge. In [10] and [11], we proposed a D-band active TA system using channel-aggregation to mitigate the design complexity and power consumption of the TX integrated circuit (IC). An off-chip substrate integrated waveguide (SIW) diplexer was used to combine two signals, with adjacent bands, output by the TX IC, so that the system covered a relative bandwidth of 11.7%, corresponding to the aggregated spectra of the two signals. However, the insertion loss of the diplexer greatly limits the overall efficiency and the maximum EIRP.

In this paper, we review our recent advances on the design of active D-band TA systems achieving enhanced efficiency thanks to an alternative channel-aggregation strategy. The two signals delivered by the TX IC are separately radiated by dedicated elements of the focal-plane antenna module. They are recombined by the TA which is optimized to ensure a high EIRP in the link direction over the entire frequency range (139.3-156.6 GHz). Both the primary source and the flat lens are fabricated using a low-cost printed circuit board (PCB) technology. We reported in [12] designs similar to one described here to demonstrate short-range high-data-rate transmission. In this work, we present an extensive characterization of the active antenna system in terms of transmitted power, radiation patterns and bandwidth. Moreover, we quantitatively compare the proposed over-the-air channel-aggregation architecture to the design in [10], showing that it increases the EIRP by about 10 dBm. Finally, we report for the first time an experimental characterization of the antenna gain of the active source and of the full system.

II. Antenna Architecture and Design

The antenna system is composed of an active primary source antenna and a flat discrete lens at a distance of 25 mm. The TX IC has been fabricated in a 45-nm CMOS silicon-on-insulator (SOI) technology and flip-chipped on the PCB with the antenna sources. The system architecture is illustrated in Fig. 1a. The IC, described in [12], comprises two up-conversion lanes with power amplifiers. Each lane is fed by an intermediate-frequency (IF) signal spanning in a band of 8.64 GHz centered at 61.56 GHz. The IC outputs two D-band signals with adjacent spectra and same bandwidth (8.64 GHz). The lower-band (LB) signal is centered at 143.34 GHz, whereas the upper-band (UB) one at 152.28 GHz. Each IC output excites a 2×1 patch array, which radiates the corresponding signal. Therefore, the spatial and frequency aggregation of LB and UB signals is performed by the TA, which collimates both in the desired link direction ($\theta = 0°$). This approach significantly differs from that demonstrated in [10], which uses a diplexer to combine the signals before the aggregated signal is radiated by a 2×2 patch array, as shown in Fig. 1b.

978-88-31299-09-1/24/$31.00 ©2024 IEEE

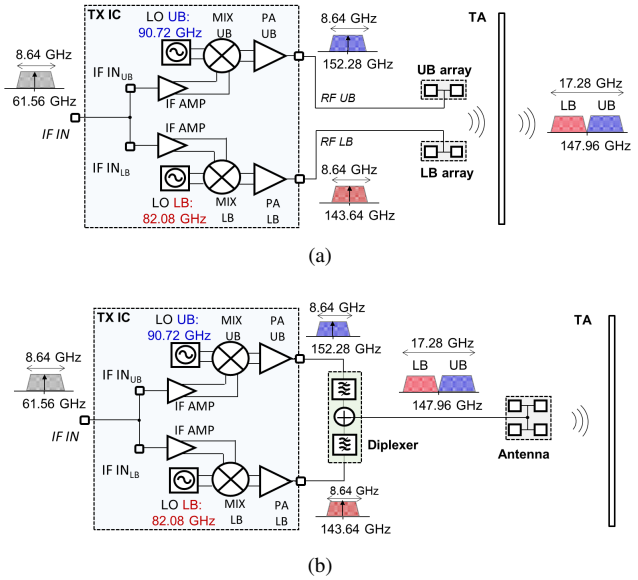

Fig. 1. Block diagram of: (a) the proposed active TA system, including separate sources for LB and UB signals; (b) the system reported in [10], which aggregates LB and UB signals using a diplexer.

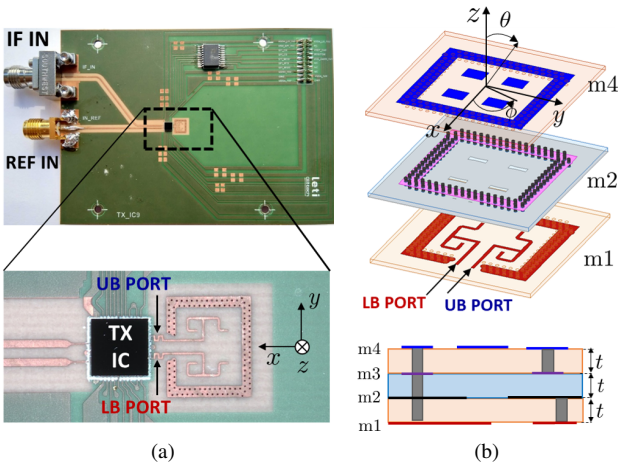

Fig. 2. (a) Picture of the bottom side of the focal-plane antenna module, with a zoom on the IC and the microstrip feeds of the LB and UB patches. (b) Exploded view and stack-up of the patch antennas. The thickness of substrate and bonding layer is $t = 0.127$ mm.

A. Focal-plane Antenna Design

The design of the primary antennas has been partially presented in [12]. A picture of the bottom side of the focal-plane module is reported in Fig. 2a. The inset shows the two outputs of the TX and the microstrip feeds of the LB and UB patch pairs. The PCB is realized using two Isola Astra MT77 substrates and a bonding layer with similar properties ($\epsilon_r = 3$, $\tan\delta = 1.7 \times 10^{-3}$) and comprises four metal layers. The patch elements on the top metal layer (*m4*) are aperture-fed by the microstrip lines in *m1* through the slots in the ground plane *m2*, as shown in Fig. 2b. They are identical and their center-to-center spacing is 1.25 mm along both $x-$ and $y-$axis. A single via-fence cavity of size 2.9 mm $\times$ 3.3 mm has been realized around the four antennas to avoid significant losses due to surface waves. The centers of LB and UB arrays are offset by 0.675 mm with respect to the symmetry axis of the antennas (x-axis). Therefore, the maximum of the radiation patterns of the two arrays does not occur at $\theta = 0°$. The full-wave simulations, performed using Ansys Electronics Desktop 2022, show that the maximum of the yz-plane pattern at 148 GHz is at $\theta = \mp 18°$ when the LB or the UB is excited, respectively. The simulated gain at $\theta = 0°$ is about 1.3 dB lower than the peak value, at each frequency. Their average values in the LB and UB are 7.3 dBi and 7.6 dBi, respectively.

B. Transmitarray Design

The unit-cells (UCs) of the TA have been been presented in part in [11]. Their structure is illustrated in Fig. 3a. They comprise only 3 metal layers, two substrates and a bonding film with the same dielectric properties of those used for the focal-plane antenna. The outer layers are orthogonal wire grid polarizers, whereas the element on the inner layer is designed to convert the incident x-polarized field in a y-polarized field introducing a desired phase shift with a minimum insertion loss. Sixteen different cells were optimized so that the phases of their transmission coefficients achieve a broadband and almost uniform 4-bit quantization of the 2π-phase range. The UCs are square, with periodicity $p = 0.75$ mm, and differ only for the inner layer. They were designed using parametric variations of the three types of rotating elements shown in Fig. 3a, with the aid of the equivalent circuits presented in [8] and full-wave simulations. Eight UCs were obtained by mirroring with respect to the y-axis the rotating elements designed for the first 8 UCs. The UCs were analyzed in simulations enforcing periodic boundary conditions and under normal plane-wave incidence. The phase shifts of the transmission coefficients of 15 UCs with respect to the phase of a reference UC are plotted in Fig. 3b. The insertion losses of all UCs are less than 1 dB from 125 GHz to 160 GHz.

The size of the TA, its phase profile and the focal length F were optimized to obtain a realized gain of at least 25 dBi at $\theta = 0°$, in both the LB and UB, and maximize the aperture efficiency. The design was carried out with an in-house numerical tool [13], which uses geometrical optics, the simulated far-field pattern of the primary source and of the UCs, and the scattering parameters of the UCs, to compute the far field and gain of the overall TA system, at each frequency. Eventually, a $17.8\lambda_0 \times 17.8\lambda_0$ TA (48×48 UCs), was designed, where λ_0 is the wavelength in vacuum at 148 GHz. The focal distance was set to $F = 25$ mm. The spatial distribution of the phase shifts introduced by the UCs is shown in Fig. 3c. It was optimized to radiate a broadside beam at 148 GHz, i.e. at the border between LB and UB, considering that the LB and UB sources are excited at the same time. With this choice, a small deviation ($< 1.6°$) of the maximum of the radiated beam with respect to the link direction ($\theta = 0°$) is attained in both LB and UB. The maximum gain drop at $\theta = 0°$ with respect to the peak value is 2.6 dB at 155 GHz.

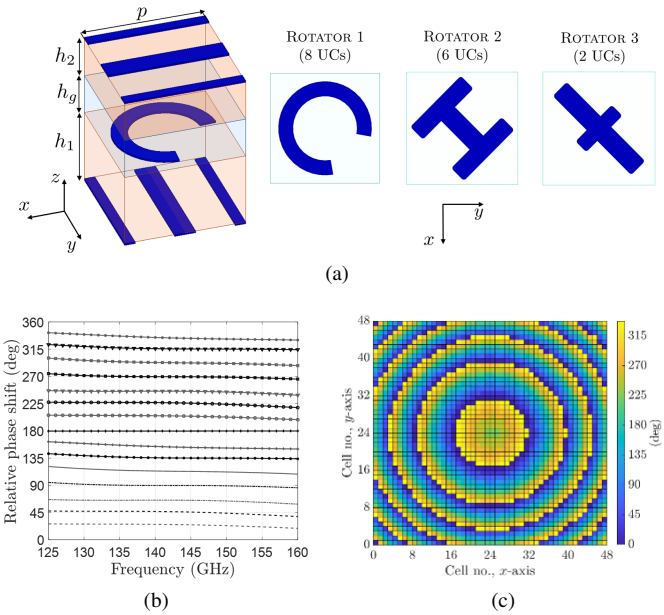

Fig. 3. (a) Structure and stack-up of the 16 UCs, with $h_1 = 0.254$ mm and $h_g = h_2 = 0.127$ mm. The 3 rotating elements used for the design of the UCs are also shown. (b) Simulated phase shift introduced by each UC with respect to that of the first one. (c) Optimized TA phase distribution.

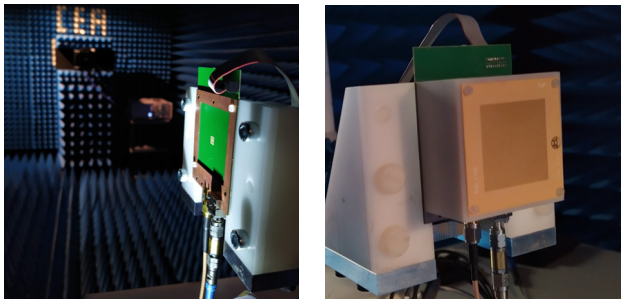

Fig. 4. Pictures of the (a) focal-plane module and (b) full system .

III. Experimental Results

The active primary source and the overall antenna system with the TA were characterized in an anechoic chamber at CEA-Leti (see Fig. 4), at the output 1-dB compression point of the TX IC. The power P_{RX} received at a distance $r_0 = 3.1$ m from each antenna under test (AUT) was measured using a standard D-band horn with a boresight gain $G_{RX} \approx 20$ dBi, a VDI-SAX down-converter and a spectrum analyzer. The power at the receiver was measured as a function of elevation angle θ in the xz- and yz-plane, respectively, by rotating the AUT with a two-axis positioner, as well as a function of frequency. To this end, the TX IC was excited by a sweeping input single-tone IF signal (see Fig. 1a). In this way, for each input tone, the performance of the AUT was simultaneously characterized at the corresponding up-converted D-band tones in the LB and UB, respectively.

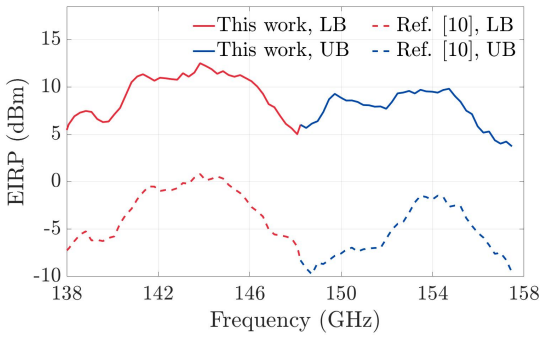

Fig. 5. Measured EIRP at $\theta = 0°$ against frequency of the proposed focal-plane antenna and of that presented in [10] (see Fig. 1b).

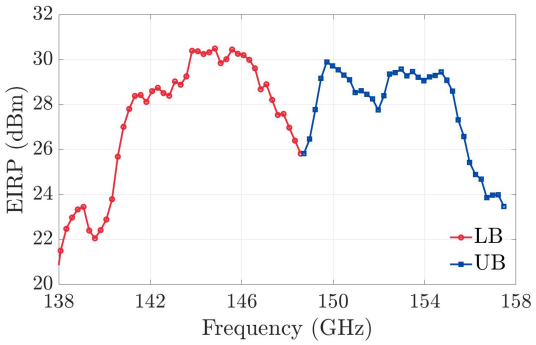

Fig. 6. Measured EIRP at $\theta = 0°$ of the TA antenna system against frequency.

A. Measured EIRP and Radiation Patterns

The values of the EIRP were evaluated from the measured power at the receiver, for each angular position (θ, ϕ) of the AUTs, using the following formula:

$$EIRP_{AUT}(\theta, \phi, f) = \left(\frac{4\pi r_0}{\lambda}\right)^2 \frac{P_{RX}(\theta, \phi, f)}{G_{RX}}, \quad (1)$$

where λ is the wavelength in free space at the frequency f, and $\phi = \{0°, 90°\}$. The path loss at 140 GHz is about 65 dB.

The measured EIRP of the proposed focal-plane antenna along the link direction $\theta = 0°$ is plotted in Fig. 5. The average difference of about 2.5 dBm between the values in the LB and the UB is mainly determined by the frequency variation of the power delivered by the IC to the antennas. This variation is due to the frequency response of the IC and to the different mismatch at the two IC outputs, which is partly affected by the flip-chip assembly and fabrication tolerances.

Fig. 5 shows also the EIRP of the focal-plane antenna that we presented in [10], which is fed by the same IC, uses a diplexer to combine LB and UB signal, and comprises a broadside 2×2 array of patches similar to those used in this work (see Fig. 1b). Compared to the latter module, the proposed prototype achieves an EIRP about 10 dBm higher, in both LB and UB. This enhancement is achieved despite the deviation of its angle of maximum radiation with respect to the link direction, due to the offset of the LB and UB sources.

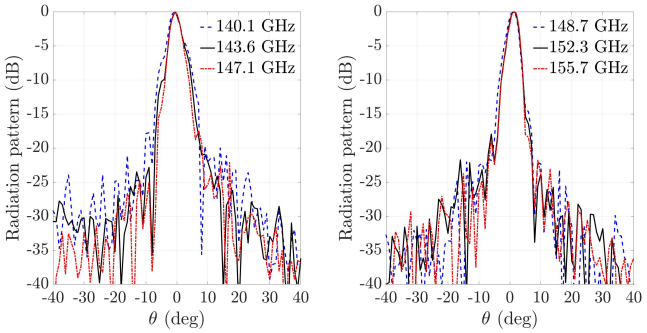

Fig. 7. Measured yz-plane cuts of the radiation patterns of the active TA system, at several frequencies in the (a) LB and (b) UB.

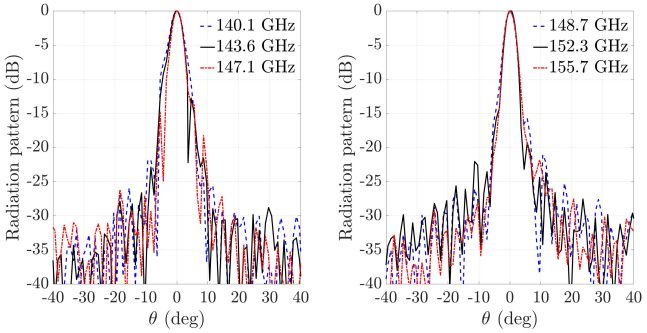

Fig. 8. Measured xz-plane cuts of the radiation patterns of the active TA system, at several frequencies in the (a) LB and (b) UB.

Indeed, the gain losses introduced by this beam tilt and by the use of 2 antennas per band instead of 4 are much lower than the insertion losses of the diplexer of the antenna in [10].

The EIRP measured at $\theta = 0°$ when the primary source illuminates the TA is plotted in Fig. 6. It attains a peak value of 30.5 dBm at 145 GHz and it is > 25 dBm from 140 GHz to 156 GHz. The dip at 148 GHz is due to the reduced output power of the IC at the edge between LB and UB.

The measured radiation patterns of the active TA system are shown, at several frequencies, in Fig. 7 (yz-plane cut) and Fig. 8 (xz-plane cut). They are plotted for $\theta \in [-40°, 40°]$, for better readability. Each pattern is normalized to its maximum. The yz-plane patterns point at negative and positive angles in the LB and UB, respectively, since the corresponding antenna sources are oppositely offset with respect to the TA center. Nevertheless, the observed scan angle is relatively small. It varies from $-1.1°$ to $-0.8°$ in the LB (Fig. 7a), and from $1°$ to $1.5°$ in the UB (Fig. 7b). The maximum difference between the pattern peak value and the value at $0°$ is 1.8 dB, from 138 GHz to 158 GHz. On the other hand, all measured xz-plane patterns (see Fig. 8) have a maximum for $\theta = 0°$, in both the LB and UB. The radiation patterns do not significantly vary with frequency in each sub-band.

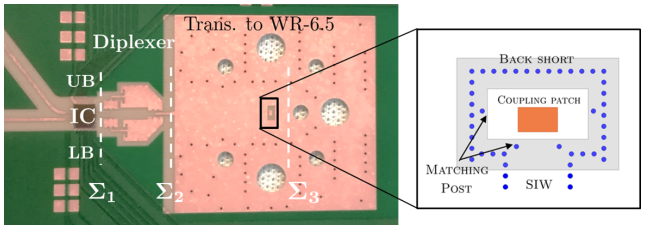

Fig. 9. Picture of the test board used to evaluate the output power of the IC at the LB and UB ports, at section Σ_1, and detail of the transition to rectangular waveguide. The 20-dBi horn vertically connected to the board is not shown.

B. Antenna Gain Characterization

The power delivered by the IC to the input lines of the LB and UB arrays could not be directly measured on the prototype. We present here an indirect technique to estimate it and the antenna gain, using the test board shown in Fig. 9. The test board has the same stack-up of the focal-plane antenna module. The input lines for the IF signals and the TX IC are nominally identical too. The two IC outputs excite the input ports of a SIW diplexer. The aggregated signal at the output of the diplexer is guided to a 20-dBi standard-gain horn, vertically assembled on the board, through a dedicated transition to a rectangular waveguide (WR-6.5). More details about the design of this board are given in [10].

The boresight EIRP ($EIRP_{test}$) of the test board has been characterized with the same experimental setup used for the active TA system. The measured scattering parameters of the stand-alone diplexer and of the transition were reported in [10]. Neglecting the mismatch at the interface Σ_2 (see Fig. 9), the power $P_{d,IC}$ delivered by the IC to the LB and UB lines can be approximately evaluated using the following formula:

$$P_{d,IC}(f) = \frac{EIRP_{test}(f)}{G_{horn}(f)} \cdot L_{tran}(f) \cdot L_{dipl}(f) \qquad (2)$$

where G_{horn} is the gain of the horn of the test board, L_{tran} is the measured insertion loss of the transition, and L_{dipl} is the measured insertion loss from the pertinent input port (LB or UB) to the output port of the diplexer.

Assuming that the values of the power delivered by the IC to the LB and UB ports of the proposed active focal-plane antenna are equal to $P_{d,IC}(f)$, the gain of the proposed antenna systems (with and without TA) in the link direction can be easily calculated as:

$$G_{AUT}(\theta = 0°, f) = \frac{EIRP_{AUT}(\theta = 0°, f)}{P_{d,IC}(f)}. \qquad (3)$$

The gain at $\theta = 0°$ of the primary source and of the TA system, obtained with this experimental method, are plotted against frequency in Fig. 10. The estimated gain of the focal-plane antenna (see Fig. 10a) oscillates around the values obtained from a full-wave simulation of the isolated antenna (see Fig. 2b). In the simulation, only one of the two input ports (LB or UB) is excited at a time, depending on whether the considered frequency is in the LB or UB, while the other one is terminated on a matched load.

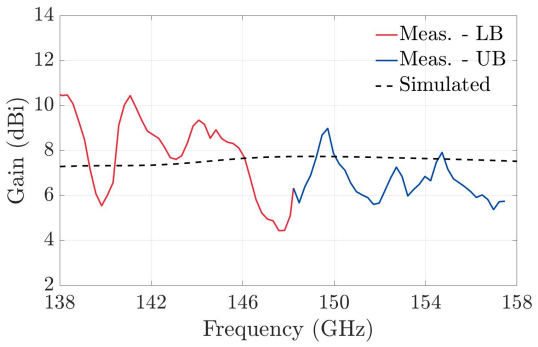

(a)

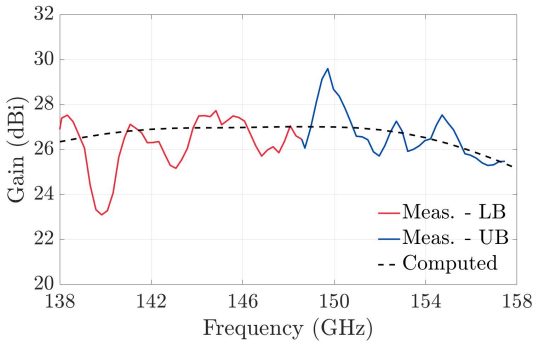

(b)

Fig. 10. Antenna gain at $\theta = 0°$ of the: (a) focal-plane antenna; (b) the overall TA system. Experimental and numerical results are compared.

The estimated gain of the complete system is in very good agreement with the values predicted by the in-house numerical code used for the analysis and optimization of the TA. The average measured gain between 138 GHz and 158 GHz is about 26 dBi.

The observed oscillations of the experimental data are due to the simplifying assumptions of the proposed technique. In particular, the estimation of the power delivered by the IC on the test board is affected by possible mismatches at the section Σ_2 or at the input of the horn, that have been neglected. Moreover, the impedances seen at the LB and UB outputs of the IC in the test board may differ from the corresponding values in the active primary source, in part as a consequence of the variability of the flip-chip assembly process.

IV. Conclusion

We have presented the design and measured performance of an efficient D-band active TA system. The focal-plane antenna radiates, with two separate pairs of patches, two signals with adjacent bands, provided by a TX IC. A 48×48-element flat discrete lens has been optimized to form a directive beam and attain a high EIRP at the direction $\theta = 0°$, in the entire frequency band covered by the two signals (139.3-156.6 GHz). Thanks to this channel-aggregation solution, the measured EIRP of the primary source is about 10 dBm higher than that demonstrated in [10] using a diplexer to combine the signals and both pairs of patches to radiate the aggregated signal. Moreover, with respect to [10], the focal length has been reduced from 30 mm to 25 mm. The measured EIRP of the full TX system at $\theta = 0°$ is higher than 25 dBm in an 11%-relative bandwidth and has a peak value of 30.5 dBm. An experimental technique to characterize the antenna gain of the primary source and of the entire TA has been described. The obtained values are in line with the numerical results. The estimated average gain of the TA in the link direction is about 26 dBi in the operating band.

References

[1] D. del Rio et al., "A D-band 16-element phased-array transceiver in 55-nm BiCMOS," *IEEE Trans. Microw. Theory Techn.*, vol. 71, no. 2, pp. 854-869, Feb. 2023.

[2] A. Ahmed, L. Li, M. Jung and G. M. Rebeiz, "A 140 GHz scalable on-grid 8×8-element transmit-receive phased-array with up/down Converters and 64QAM/24 Gbps data rates," in *Proc. IEEE Radio Freq. Integr. Circuits Symp. (RFIC)*, San Jun. 2023, pp. 93-96.

[3] A. A. Farid, A. S. H. Ahmed, A. Dhananjay and M. J. W. Rodwell, "A fully packaged 135-GHz multiuser MIMO transmitter array tile for wireless communications," *IEEE Trans. Microw. Theory Techn.*, vol. 70, no. 7, pp. 3396-3405, July 2022.

[4] M. Arias Campo et al., "H-Band quartz-silicon leaky-wave lens with air-bridge interconnect to GaAs front-end," *IEEE Trans. THz Sci. Tech.*, vol. 11, no. 3, pp. 297-309, May 2021.

[5] A. Dyck et al., "A transmitter system-in-package at 300 GHz with an off-chip antenna and GaAs-based MMICs," *IEEE Trans. THz Sci. Tech.*, vol. 9, no. 3, pp. 335-344, May 2019.

[6] Z.-W. Miao, Z. C. Hao, Y. Wang, B.-B. Jin, J.-B. Wu and W. Hong, "A 400-GHz high-gain quartz-based single layered folded reflectarray antenna for terahertz applications," *IEEE Trans. THz Sci. Tech.*, vol. 9, no. 1, pp. 78-88, Jan. 2019

[7] S. Venkatesh et al., "A high-speed programmable and scalable terahertz holographic metasurface based on tiled CMOS chips," *Nat. Electron.*, vol. 3, pp. 785–793, 2020.

[8] O. Koutsos, F. Foglia Manzillo, A. Clemente and R. Sauleau, "Analysis, rigorous design, and characterization of a three-layer anisotropic transmitarray at 300 GHz," *IEEE Trans. Antennas Propag.*, vol. 70, no. 7, pp. 5437-5446, July 2022.

[9] O. Koutsos, F. Foglia Manzillo, M. Caillet, R. Sauleau and A. Clemente, "Experimental demonstration of a 43-dBi gain transmitarray in PCB technology for backhauling in the 300-GHz band," *IEEE Trans. THz Sci. Techn.*, vol. 13, no. 5, pp. 485-492, Sept. 2023.

[10] A. Hamani et al., "A D-band multichannel TX system-in-package achieving 84.48 Gb/s with 64-QAM based on 45-nm CMOS and low-cost PCB technology," *IEEE Trans. Microw. Theory Techn.*, vol. 70, no. 7, pp. 3385-3395, Jul. 2022.

[11] F. Foglia Manzillo, A. Hamani, A. Siligaris, A. Clemente and J. L. Gonzalez-Jimenez, "A highly directive D-band antenna module comprising a flat discrete lens and an active feed," in *Proc. IEEE Int. Symp. Antennas Propag. (AP-S/URSI)*, Jul. 2022, pp. 321-322.

[12] J. L. Gonzalez-Jimenez et al., "A 57.6 Gb/s wireless link based on 26.4 dBm EIRP D-band transmitter module and a channel bonding chipset on CMOS 45nm," in Proc. *Proc. IEEE Radio Freq. Integr. Circuits Symp. (RFIC)*, Jun. 2023, pp. 97-100.

[13] H. Kaouach et al., "Wideband low-loss linear and circular polarization transmit-arrays in V-band," *IEEE Trans. Antennas Propag.*, vol. 59, no. 7, pp. 2513–2523, 2011.